Yang et al. Nanoscale Research Letters (2016) 11:233
DOI 10.1186/s11671-016-1447-0

Nanoscale Research Letters

NANO EXPRESS Open Access

Enhanced Photoelectrical Response of Hydrogenated Amorphous Silicon Single-Nanowire Solar Cells by Front-Opening Crescent Design

Zhenhai Yang[1,2†], Guoyang Cao[1,3†], Aixue Shang[1,3], Dang Yuan Lei[4], Cheng Zhang[1,3], Pingqi Gao[2*], Jichun Ye[2] and Xiaofeng Li[1,3*]

Abstract

We report an approach for substantially enhancing the light-trapping and photoconversion efficiency of hydrogenated amorphous silicon (a-Si:H) single-nanowire solar cells (SNSCs) by engineering the cross section of the nanowire from circular into a front-opening crescent shape. The proposed SNSCs show a broadband and highly tunable optical absorption compared to the conventional circular counterparts under both transverse electric and transverse magnetic incidences, enabling an enhancement ratio of over 40 % in both the photocurrent density and the photoconversion efficiency in a-Si:H SNSCs with a diameter of 200 nm. We further show that the superior performance can be well maintained under a wide range of incident angle and is robust to the blunt crescent edges.

Keywords: Single-nanowire solar cells, Coupled optoelectronic simulation, Light-trapping, Crescent

PACS: 85.60.-q, Optoelectronic device, 84.60.Jt, Photovoltaic conversion

Background

Single semiconductor nanowires (NWs) have been explored extensively over the past decades due to their unique nanoscale morphology and outstanding photoelectric response, which can find a variety of potential applications, e.g., photovoltaics (PV) [1–4], photodetectors/sensors [5–7], light-emitting diodes [8–10], and thermoelectric devices [11–13]. Particularly, compact single-nanowire solar cells (SNSCs) have attracted considerable attention due to their excellent light-trapping ability, efficient carrier collection, and convenient integration into chips. However, the potential of SNSCs in realizing highly efficient nanoscale PV devices has not been fully exploited. From the fundamental light-trapping to the intrinsic photoconversion processes, there still exist many challenges. In order to improve the light-trapping performance, coaxial heterojunction [14, 15], dielectric-shell coating [16, 17], rear reflector [18, 19], and metal-core/semiconductor-shell NWs [20, 21] have been proposed. In electrical perspectives, photocurrent matching (for double-junction SNSCs) [15], electrical doping, recombination loss [22], etc. have to be carefully addressed as well.

Among various performance-modulation strategies, optimizing the cross-sectional morphology of NWs is an easy way to enhance the light-harvesting response [23–26]. For instance, Kim et al. showed that the rectangular silicon NWs have enhanced external quantum efficiency (EQE) than their circular counterparts at long wavelengths [23]. Cao et al. proposed a series of SNSCs with various cross sections including circle, square, hexagon, and triangle, which, however, seem to display similar optical response if taking the volume difference into account [24]. We recently found that the light-trapping ability of silicon-based SNSCs can be significantly

* Correspondence: gaopingqi@nimte.ac.cn; xfli@suda.edu.cn
†Equal contributors
[2]Ningbo Institute of Material Technology and Engineering, Chinese Academy of Sciences, Ningbo 315201, China
[1]College of Physics, Optoelectronics and Energy & Collaborative Innovation Center of Suzhou Nano Science and Technology, Soochow University, Suzhou 215006, China
Full list of author information is available at the end of the article

improved by introducing the symmetry-broken rear-crescent design, benefitted from the dramatically enhanced absorption peaks, especially in the long-wavelength band [26].

In this study, we focus on the application of crescent configuration in improving the light-trapping and photo-conversion performance of SNSCs consisted of highly absorbing hydrogenated amorphous silicon (a-Si:H). We consider different crescent orientations against the solar incidence as well as the comparison between the crescent and the conventional circular systems. Finite-element method (FEM) and carrier-transport calculations are employed to predict the optical and electrical performance of the a-Si:H SNSCs, respectively. The absorption patterns under various cavity resonances are used to uncover the physics behind the performance enhancement. It shows that the photocurrent density (J_{ph}) can be increased from 14.38 to 20.22 mA/cm^2 by the optimized crescent design when comparing the circular counterpart; moreover, the outstanding light-harvesting capability can be well sustained in a wide range of incident angle or with the presence of blunt crescent tips. Simulation on carrier transportation and collection predicts an enhancement ratio of 43.77 % in light-conversion efficiency over the circular system.

Methods

The cross-sectional configuration of a-Si:H SNSCs with front-opening crescent design is shown by the inset of Fig. 1b, where the NW diameter D, crescent thickness t, and vertex angle of the crescent tip θ are the key parameters to characterize the device geometry [26, 27]. The length of the lying NW is far beyond the cross-sectional sizes, allowing the two-dimensional (2D) simulation. To predict the performance of SNSCs, transverse electric (TE, electric field along the NW) and transverse magnetic (TM, magnetic field along the NW) incidences have to be considered so that the unpolarized solar incidence can be approximated as the average of TE and TM cases. The optical parameters of a-Si:H are taken from Palik's data [28]. The absorption percentage of the cell (Q_{abs}) can be obtained by solving Maxwell's equations, and an estimated (assuming perfect internal photoconversion progress) photocurrent density (J_{ph}) is obtained by spectrally integrating Q_{abs} weighted by the AM1.5G solar spectrum within the wavelength range of 300~900 nm [29, 30]. The actual electrical response (EQE, short-circuit current density (J_{sc}), current-voltage characteristics, etc.) of the SNSCs can be achieved by performing the detailed carrier transport/collection calculation, which is based on the carrier drift-diffusion and Poisson's equations coupled with Maxwell's equations. It is obvious that both J_{ph} and J_{sc} subject to unpolarized incidence should be the average of TE and TM cases. The detailed information on the coupled optoelectronic simulation can refer to our previous publications [31–35].

Results and Discussion

First of all, we focus on how to modulate the optical response of the a-Si:H SNSCs ($D = 200$ nm) by controlling the crescent parameters t and θ. Fig. 1a plots J_{ph} as a function of the tunable parameters t (100 nm < t < 160 nm) and θ (0° < θ < 85°), under an unpolarized incidence. Apparently, the value of J_{ph} shows strong dependences on both t and θ, showing that the cavity and crescent factors play very crucial roles in determining the absorption performance of the considered SNSCs. With an optimal

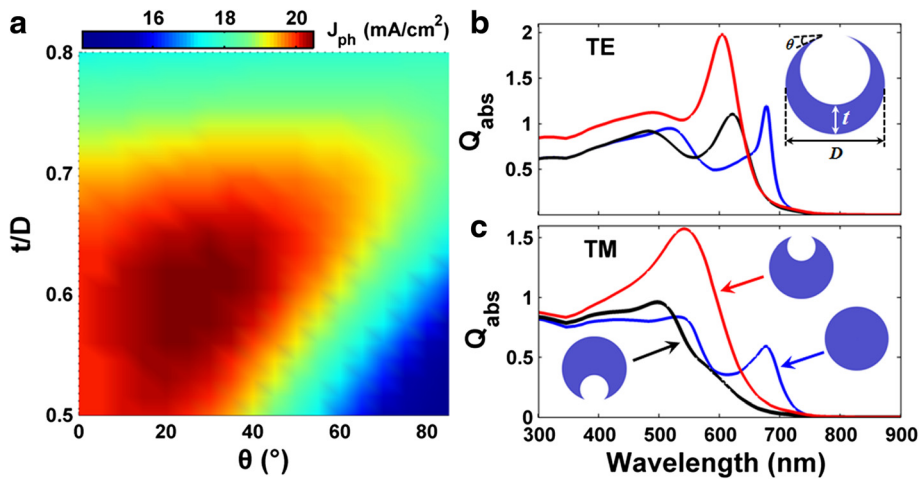

Fig. 1 Photocurrent map and absorption spectra. **a** Photocurrent density (J_{ph}) versus thickness/diameter (t/D) and vertex angle (θ) for the front-opening crescent a-Si:H SNSCs under unpolarized incidence; absorption efficiency (Q_{abs}) of the circular ($D = 200$ nm), rear- and front-opening crescent (D =200 nm, $t/D = 0.6$, $\theta = 25°$) systems for TE (**b**) and TM (**c**) incidences

crescent design, i.e., $t/D = 0.6$ and $\theta = 25°$, peaked J_{ph} exceeding 20 mA/cm^2 can be realized. Particularly, Fig. 1a also shows that there are quite wide ranges for t and θ to obtain a J_{ph}, which can be much higher than that of the conventional circular-shaped SNSCs.

Figure 1b (Fig. 1c) provides a detailed comparison of the absorption responses of the SNSCs with circular and front- and rear-opening crescent configurations under TE (TM) incidence. We first compare the rear-opening crescent and circular systems. Figure 1b indicates that under TE incidence, Q_{abs} shows an unnoticeable change in short-wavelength ($\lambda < 450$ nm) range but a strong oscillation in long-wavelength range when comparing to the circular one. Under TM incidence, however, performance enhancement (degradation) is observed when $\lambda <$ (>) 520 nm, as displayed in Fig. 1c. As a whole, under TE (TM) incidence, the J_{ph} of rear-opening crescent cells is only 14.89 (11.01) mA/cm^2, which is even lower than that based on the traditional circular system, i.e., 15.35 (13.41) mA/cm^2. Attention should be paid here on that SNSCs composed by low-absorbing crystalline silicon (c-Si) show dramatically improved J_{ph} with the rear-opening crescent design, due to the significantly enhanced cavity resonance [25, 26]. However, for the a-Si:H SNSCs which consisted of a much smaller cavity, the supported cavity modes are much less in number, so that the rear-opening crescent design can hardly play a similar effect in enhancing the absorption performance as that in the c-Si SNSCs.

On the contrary, front-opening crescent SNSCs exhibit significantly improved broadband optical absorption under both TE and TM incidences. Figure 1b, c illustrates that higher Q_{abs} can be achieved in the whole band when comparing with the rear-crescent system; the front-opening crescent system greatly outperforms the conventional circular system in a very broad spectral band (300 nm $< \lambda <$ 635 nm), leaving only a narrow band to show the slightly degraded Q_{abs}. Under the enhanced antenna effect mediated by the front-opening crescent nanostructure, the peaked Q_{abs} can be up to 1.97 (1.57) at $\lambda = 605$ nm (540 nm) under TE (TM) incidence. Ultimately, the front-opening crescent SNSCs exhibit an enhancement of 40.61 % (from 14.38 to 20.22 mA/cm^2) in J_{ph} than that of the conventional circular setup.

To reveal the physical mechanism behind the outstanding light-trapping performance by the front-opening crescent design, we examine the cross-sectional electric field distribution at several representative wavelengths corresponding to the absorption peaks in Fig. 1b, c. We first focus on the TE cases shown in Fig. 2((a_1), (b_1), (c_1)) for circular, rear-crescent, and front-crescent systems, respectively. For circular NWs, a standard whispering-gallery leaky mode is excited. Modifying the NW cross section into the rear-opening crescent, the resonant characteristics are affected significantly to show stronger peaks but with less number of hot spots (i.e., lower response order), leading to a slightly lower Q_{abs} as indicated in Fig. 1b. Nevertheless, the front-opening crescent modulation to the NW cross-section leads to substantially enhanced absorption performance in both the increased number of field hot spots as well as the increased field intensity. The physical reason lies in that the continuously varying crescent tips allows a nearly perfect impedance match between air and the cell,

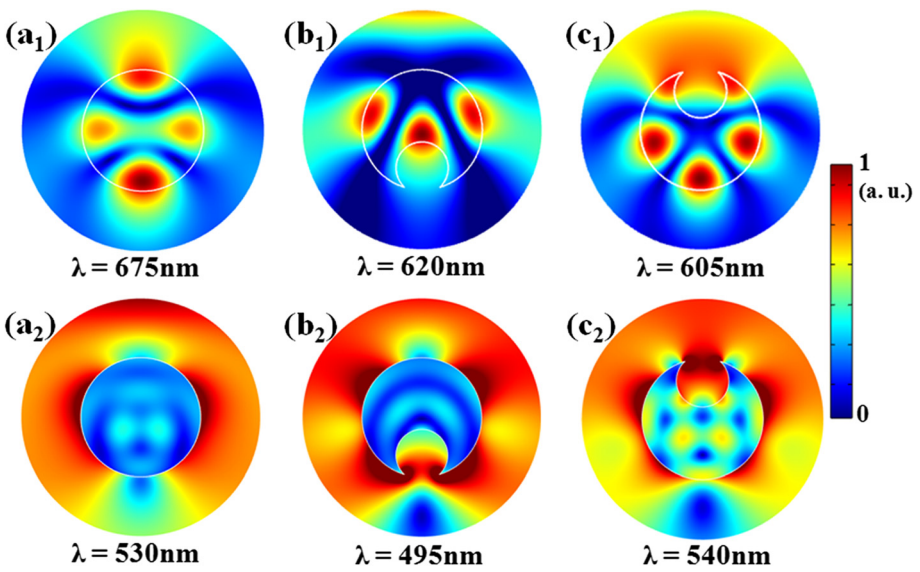

Fig. 2 Electric field patterns. Normalized electric field patterns corresponding to the peak wavelengths in Fig. 1b and c for circular (a_1)/(a_2), rear-opening crescent (b_1)/(b_2), and front-opening crescent (c_1)/(c_2) designs under TE/TM incidence

greatly suppressing the reflection and strengthening the optical antenna effect. Therefore, the high performance of the front-opening crescent a-Si:H NW is from both the impedance match as well as the strengthened cavity resonance. However, under TM incidence, the situation changes significantly. This is because the TM illumination has the electric field along the radial direction, along which the NW cavity is too small to support sufficient cavity resonances. Therefore, we could not see the distinct patterns in Fig. 2((a_2), (b_2), (c_2)). In this case, the impedance match plays an important role in coupling the incident light into the NW cavity; therefore, the front-opening crescent configuration has the born benefit in enhancing the absorption performance of SNSCs as displayed in Fig. $2c_2$.

Figure 3 plots J_{ph} versus δ (incident angle) for the optimized crescent NWs with $D = 200$ nm under TE, TM, and unpolarized incidences, respectively, where the circular system is taken to be the reference. Compared to the angle-independent circular system with $J_{ph} = 14.38$ mA/cm^2, performance is monotonously decreased in front-opening crescent a-Si:H SNSCs with increasing δ from 0° to 180° under TM incidence. Under TE incidence, performance is slightly recovered under backward incidence, but the J_{ph} value is far lower than that with normal incidence. An overall effect for the unpolarized incidence is with increasing δ, the system optical response is gradually degraded; however, the front-opening crescent design can always outperform the circular system as long as $\delta < 90°$, which is the case for the most PV systems. Therefore, high optical performance can be sustained under a very wide range of the incident angle by employing the front-opening crescent cross-sectional design for SNSCs.

We now examine the tunability of the front-opening crescent a-Si:H SNSCs. Figure 4a, b displays the dispersion characteristics under TE and TM incidences, respectively. In these calculations, $t/D = 0.6$ and $\theta = 25°$ are used to guarantee a constant geometrical morphology. With increasing D, it is observed that (1) more high-order optical cavity modes are excited, with the lower-order modes being degenerated/disappearred (the electric field patterns for the resonant modes marked in the figures are displayed on the right side, i.e., patterns A–D and I–IV); (2) the resonant wavelengths are red-shifted distinctly; (3) absorption band is increased but the peaked absorption is decreased; and (4) the strong absorption appears when D is relatively small, i.e., the lower-order modes contribute high absorption. Therefore, the strong sensitivity of the absorption performance on the NW size facilitates the control and optimization of the optical response. Figure 4c displays the optimized J_{ph} versus D for circular and crescent SNSCs under the unpolarized incidence. It is seen that with D <100 nm, the circular cell is relatively more capable in light-trapping than the crescent one; however, with increasing D, the front-opening crescent system shows a much higher J_{ph}, especially when 150 nm < D < 250 nm.

In the above optical simulation, we assumed a perfect internal quantum efficiency (i.e., IQE = 100 %), which neglects all kinds of recombination in carrier transportation progress inside the solar cells. To have a comprehensive and actual evaluation on the a-Si:H SNSCs, we perform a detailed electrical simulation [26, 31–35]. The classical electrical parameters of a-Si:H are used in this model, e.g., the doping concentrations of n (p) regions are 1.3×10^{18} (1.3×10^{17}) cm^{-3}; the thicknesses of $p/i/n$ regions are 40/20/40 nm. The rest parameters including

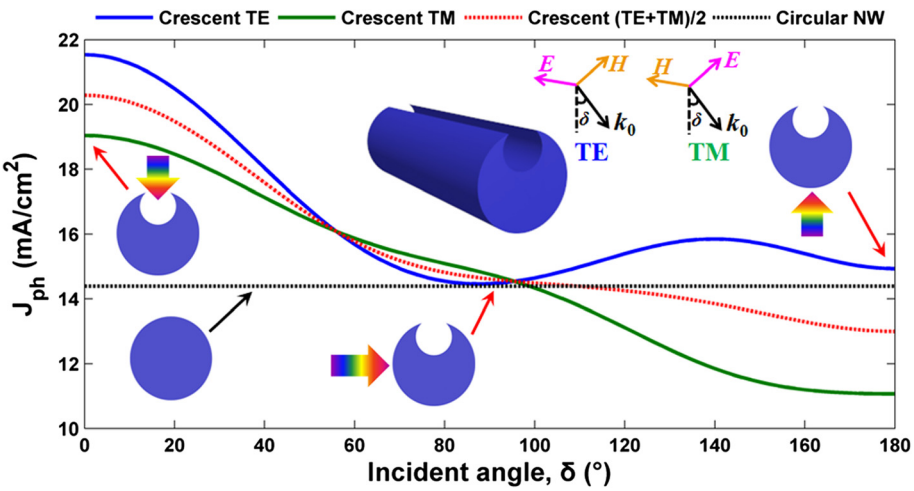

Fig. 3 Photocurrent densities. Photocurrent density (J_{ph}) versus incident angle (δ) for the circular and optimized front-opening crescent designs. The *insets* are the schematic diagrams under various cell configurations

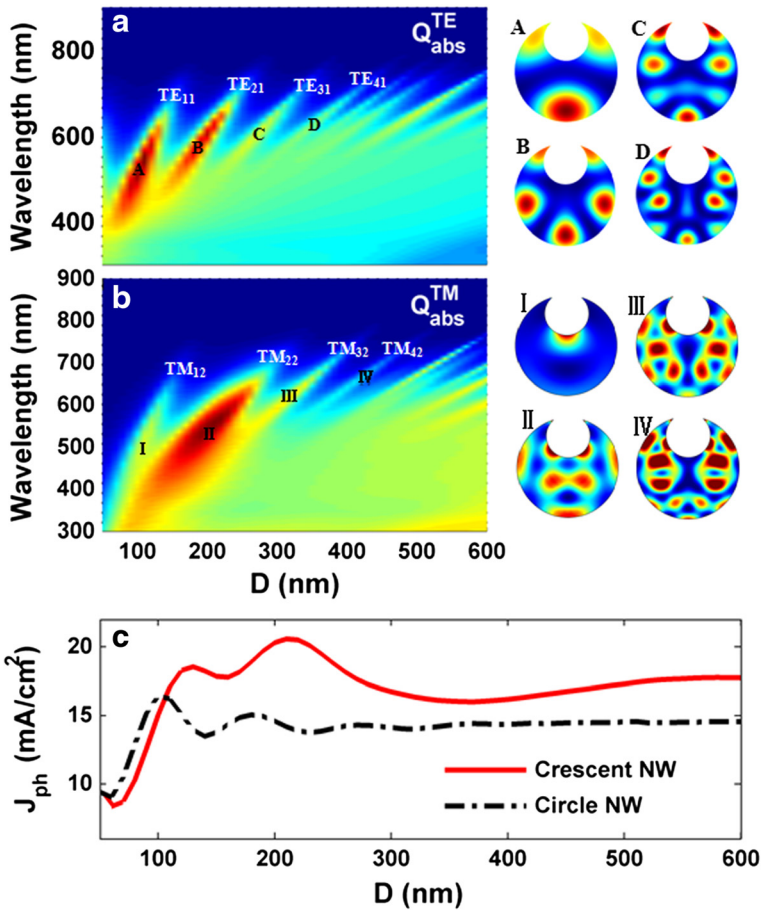

Fig. 4 Absorption spectra and electric field patterns. Absorption spectrum (Q_{abs}) versus D under TE (**a**) and TM (**b**) incidences; **c** photocurrent density (J_{ph}) versus D. The electric field patterns of the resonant modes are inserted into the figure

intrinsic carrier concentration, carrier mobility, lifetime, and recombination coefficients can be found in reference [35]. Furthermore, two electrodes that are shown in the inserted device schematic in Fig. 5a are employed as perfect ohmic contacts. In this study, we neglect the effect of the collector contacts since the NW length is far beyond than its diameter, leaving a very small portion covered by the electrodes.

Figure 5a shows the simulated EQE spectra of the optimized front-opening crescent and circular a-Si:H SNSCs under an unpolarized incidence. Apparently, realistic carrier transportation process would bring recombination loss for incidences under all wavelengths, leading EQE to be slightly lower than that of Q_{abs}. As a result, photocurrent density (see the inserted table in Fig. 5b) is reduced from $J_{ph} = 20.22$ (14.38) mA/cm^2, i.e., integration of Q_{abs} under AM1.5G, to $J_{sc} = 19.26$ (13.58) mA/cm^2, i.e., integration of EQE under AM1.5G, for crescent(circular) a-Si:H SNSCs. Figure 5b plots the current-voltage (J-V) curves of these two types of a-Si:H SNSCs. Apart from J_{sc}, the proposed device exhibits a slightly increased open-circuit voltage V_{oc} (from 923 to 945 mV), a similar fill factor (FF) (i.e., 87.12 and 86.26 %), and a significantly increased light-conversion efficiency (η) from 10.92 to 15.70 % (enhancement ratio is 43.77 %), compared to traditional circular system.

Finally, it is necessary to examine the detailed electronic response of the SNSCs under crescent design since the device has an increased surface area which might lead to a higher surface recombination. Our study indicates that the detailed simulation of the intrinsic carrier transport/recombination processes enables a more accurate prediction on the photocurrent of the device, i.e., the photocurrent is 0.8 (0.96) mA/cm^2 lower than that based on the purely optical estimation (assuming the lossless internal quantum process) for circular (crescent) SNSCs. The crescent SNSCs exhibits a relatively larger photocurrent loss, revealing a higher carrier recombination. To further explore the recombination processes, Fig. 6a, b quantifies the photocurrent losses due to the bulk and surface recombinations, respectively. It is obvious that the circular SNSCs have a stronger

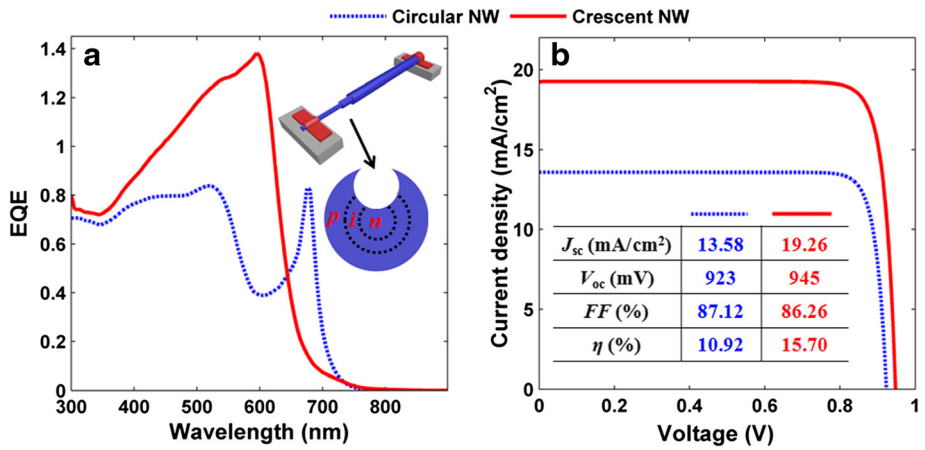

Fig. 5 EQE spectra and *I-V* characteristics. **a** EQE spectra and (**b**) *I-V* characteristics of the front-opening crescent a-Si:H SNSCs with $D = 200$ nm. The device schematic and the tabulated electrical parameters are inserted in (**a**) and (**b**), respectively

bulk recombination due to the larger device volume; however, the crescent SNSCs exhibit much higher photocurrent loss by surface recombination due to the increased surface area. The combined effect by bulk and surface recombinations results in comparable overall photocurrent losses (i.e., 0.8 and 0.96 mA/cm^2) by these two kinds of recombination. Therefore, despite that the cell surface is increased by crescent design, the device electrical performance can be well sustained. Moreover, we would like to indicate that the ideally poignant crescent tips have been used in the previous simulations. To take account of the manufacturing capabilities, the blunt tips have to be considered [27]. In our simulations, we have examined the effect of the blunt tips on the absorption performance. It is found that the blunt tips do not qualitatively impact the value of J_{ph}, i.e., under a representative blunt configuration, J_{ph} under TE (TM) incidence is 21.18 (19.10) mA/cm^2, which is just slightly lower than that of the poignant case, i.e., 21.48 (18.96) mA/cm^2, showing an average decrement less than 0.40 %.

Conclusions

In summary, we proposed a design of a-Si:H-based SNSCs with front-crescent cross-sectional morphology in order to obtain broadband and strong optical absorption for efficient photoconversion. By electromagnetic and carrier-transport calculation, we comprehensively evaluated the optoelectronic performance of the crescent a-Si:H SNSCs. Comparisons of front-opening crescent, rear-opening crescent, and conventional circular a-Si:H SNSCs were given under TE, TM, and unpolarized incidences. It was found that the photocurrent density of the front-opening crescent SNSCs can be improved by over 40 % relative to the conventional circular design due to the improved impedance-matching condition as well as the enhanced optical antenna effect. This design has a good tolerance against the change of the incident

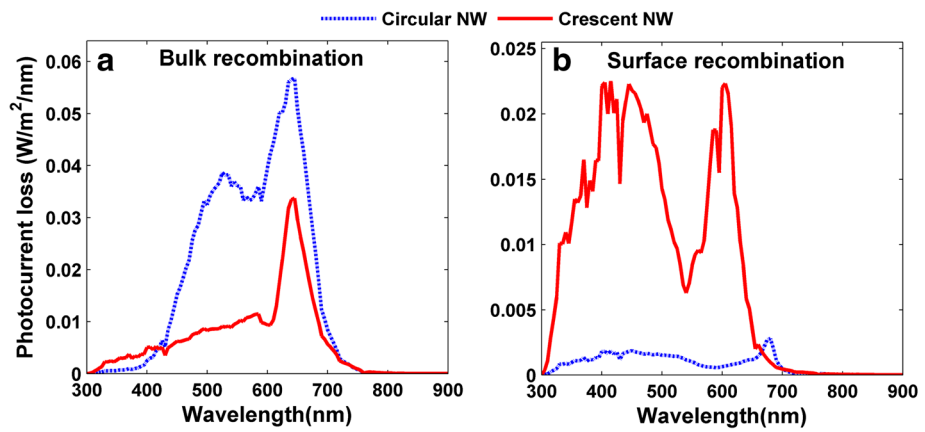

Fig. 6 Photocurrent density losses by carrier recombinations. Current density losses arisen from (**a**) bulk and (**b**) surface recombinations for the circular and optimized front-opening crescent designs, respectively

angle and a high tunability on the optical resonance. Electrical simulation forecasted that the light-conversion efficiency can be up to 15.70 %, showing an enhancement ratio of 43.77 % relative to the circular counterparts.

Abbreviations

EQEs: external quantum efficiencies; FEM: Finite-element method; FF: fill factor; IQE: internal quantum efficiency; J_{ph}: photocurrent density; J_{sc}: short-circuit current density; *J-V*: current-voltage; NWs: nanowires; SNSCs: single-nanowire solar cells; TE: transverse electric; TM: transverse magnetic; V_{oc}: open-circuit voltage.

Competing Interests

The authors declare that they have no competing interests.

Authors' Contributions

ZY and GY carried out the study design and drafted the manuscript. XL conceived the design and supervised the research. AS participated in the *I-V* simulation. DY, CZ, PG, and JY commented on the results and revised the manuscript. All authors read and approved the final manuscript.

Acknowledgements

This work was supported by Ph.D. Programs Foundation of Ministry of Education of China (20133201110021), Youth 973 Program (2015CB932700), "Thousand Young Talents Program" of China, Priority Academic Program Development (PAPD) of Jiangsu Higher Education Institutions, National Natural Science Foundation of China (61404144), and Zhejiang Provincial Natural Science Foundation (LY14F040005). DYL acknowledges the support by the Hong Kong Research Grants Council (ECS Grant no. 509513).

Author details

[1]College of Physics, Optoelectronics and Energy & Collaborative Innovation Center of Suzhou Nano Science and Technology, Soochow University, Suzhou 215006, China. [2]Ningbo Institute of Material Technology and Engineering, Chinese Academy of Sciences, Ningbo 315201, China. [3]Key Lab of Advanced Optical Manufacturing Technologies of Jiangsu Province and Key Lab of Modern Optical Technologies of Education Ministry of China, Soochow University, Suzhou 215006, China. [4]Department of Applied Physics, The Hong Kong Polytechnic University, Hong Kong, China.

Received: 27 February 2016 Accepted: 20 April 2016
Published online: 29 April 2016

References

1. Tian B, Zheng X, Kempa TJ, Fang Y, Yu N, Yu G et al (2007) Coaxial silicon nanowires as solar cells and nanoelectronic power sources. Nature 449:885–889
2. Cao L, White SJ, Park JS, Schuller JA, Clemens BM, Brongersma ML (2009) Engineering light absorption in semiconductor nanowire devices. Nat Mater 8:643–647
3. Brubaker MD, Blanchard PT, Schlager JB, Sanders AW, Roshko A, Duff SM et al (2013) On-chip optical interconnects made with gallium nitride nanowires. Nano Lett 13:374–377
4. Zhan Y, Li X, Wu S, Li K, Yang Z, Shang A (2014) Enhanced photoabsorption in top-tapered single-nanowire solar cells. Opt Lett 39:5756–5759
5. Kim CJ, Lee HS, Cho YJ, Kang K, Jo MH (2010) Diameter-dependent internal gain in ohmic Ge nanowire photodetectors. Nano Lett 10:2043–2048
6. Dai X, Zhang S, Wang Z, Adamo G, Liu H, Huang Y et al (2014) GaAs/AlGaAs nanowire photodetector. Nano Lett 14:2688–2693
7. Zhan Y, Li X, Wu K, Wu S, Deng J (2015) Coaxial Ag/ZnO/Ag nanowire for highly sensitive hot-electron photodetection. Appl Phys Lett 106:081109
8. Jiming B, Mariano AZ, Federico C (2006) Broadband ZnO single-nanowire light-emitting diode. Nano Lett 6:1719–1722
9. Fang Q, Silvija G, Yat L, Cheng Y, Charles ML (2005) Core/multishell nanowire heterostructures as multicolor, high-efficiency light-emitting diodes. Nano Lett 5:2287–2291
10. Ra YH, Navamathavan R, Yoo H, Lee CR (2014) Single nanowire light-emitting diodes using uniaxial and coaxial InGaN/GaN multiple quantum wells synthesized by metalorganic chemical vapor deposition. Nano Lett 14:1537–1545
11. Hochbaum AI, Chen R, Delgado RD, Liang W, Garnett EC (2008) Enhanced thermoelectric performance of rough silicon nanowires. Nature 451:163–167
12. Boukai AI, Bunimovich Y, Tahir-Kheli J, Yu JK (2008) Silicon nanowires as efficient thermoelectric materials. Nature 451:168–171
13. Kim R, Datta S, Lundstrom MS (2009) Influence of dimensionality on thermoelectric device performance. J Appl Phys 105:034506
14. Liu W, Oh J, Shen W (2011) Light absorption mechanism in single c-Si (core)/a-Si (shell) coaxial nanowires. Nanotechnology 22:125705
15. Cao G, Li X, Zhan Y, Wu S, Shang A, Zhang C et al (2014) Design of μc-Si:H/a-Si:H coaxial tandem single-nanowire solar cells considering photocurrent matching. Opt Express 22:A1761–A1767
16. Zhang C, Yang Z, Shang A, Wu S, Zhan Y, Li X (2015) Improved optical absorption of silicon single-nanowire solar cells by off-axial core/shell design. Nano Energy 17:233–240
17. Khudiyev T, Bayindir M (2014) Superenhancers: novel opportunities for nanowire optoelectronics. Sci Rep 4:7505
18. Jia Y, Qiu M, Wu H, Cui Y, Fan S, Ruan Z (2015) Theory of half-space light absorption enhancement for leaky mode resonant nanowires. Nano Lett 15:5513–5518
19. Wu S, Li X, Zhan Y, Li K (2014) Absorption enhancement of single silicon nanowire by tailoring rear metallic film for photovoltaic applications. Opt Lett 39:817–820
20. Zhan Y, Zhao J, Zhou C, Alemayehu M, Li YP, Li Y (2012) Enhanced photon absorption of single nanowire α-Si solar cells modulated by silver core. Opt Express 20:11507–11516
21. Shi L, Zhou Z, Huang Z (2013) The influence of silver core position on enhanced photon absorption of single nanowire α-Si solar cells. Opt Express 21:A1007–A1017
22. Zhai X, Wu S, Shang A, Li X (2015) Limiting efficiency calculation of silicon single-nanowire solar cells with considering auger recombination. Appl Phys Lett 106:063904
23. Kim SK, Day RW, Cahoon JF, Kempa TJ, Song KD, Park HG et al (2012) Tuning light absorption in core/shell silicon nanowire photovoltaic devices through morphological design. Nano Lett 12:4971–4976
24. Cao L, Fan P, Vasudev AP, White JS, Yu Z (2010) Semiconductor nanowire optical antenna solar absorbers. Nano Lett 10:439–445
25. Li X, Zhan Y (2013) Enhanced external quantum efficiency in rectangular single nanowire solar cells. Appl Phys Lett 102:021101
26. Yang Z, Li X, Lei DY, Shang A, Wu S (2015) Omnidirectional absorption enhancement of symmetry-broken crescent-deformed single-nanowire photovoltaic cells. Nano Energy 13:9–17
27. Luo Y, Lei DY, Maier SA, Pendry JB (2012) Broadband light harvesting nanostructures robust to edge bluntness. Phys Rev Lett 112:023901
28. Palik ED (1985) Handbook of optical constants of solids. Academic Press, Orlando
29. Comsol multiphysics, http://www.comsol.com/. Accessed 20 Apr 2016
30. ASTM, Reference solar spectral irradiance: AM 1.5 Spectra. http://rredc.nrel.gov/solar/spectra/am1.5. Accessed 21 Apr 2016
31. Li X, Hylton NP, Giannini V, Lee KH, Ekins-Daukes NJ, Maier SA (2013) Multi-dimensional modelling of solar cells with electromagnetic and carrier transport calculations. Prog Photovolt Res Appl 21:109–120
32. Zhan Y, Li X, Li Y (2013) Numerical simulation of light-trapping and photoelectric conversion in single nanowire silicon solar cells. IEEE J Sel Top Quantum Electron 19:4000208
33. Li X, Hylton NP, Giannini V, Lee KH, Ekins-Daukes NJ, Maier SA (2011) Bridging electromagnetic and carrier transport calculations for three-dimensional modelling of plasmonic solar cells. Opt Express 19:A888–A896
34. Li X, Zhan Y, Wang C (2015) Broadband enhancement of coaxial heterogeneous gallium arsenide single-nanowire solar cells. Prog Photovolt Res Appl 23:628–636
35. Yang Z, Shang A, Zhan Y, Zhang C, Li X (2013) Ultra-broadband performance enhancement of thin-film amorphous silicon solar cells with conformal zigzag configuration. Opt Lett 38:5071–5074